Catalysis Science & Technology

PAPER

View Article Online
View Journal | View Issue

Cite this: *Catal. Sci. Technol.*, 2018, **8**, 5003

Investigating *Saccharomyces cerevisiae* alkene reductase OYE 3 by substrate profiling, X-ray crystallography and computational methods†

Robert W. Powell, III,[a] M. Pilar Buteler,‡[a] Sunidhi Lenka,‡[a] Michele Crotti,‡[b] Sara Santangelo,‡[b] Matthew J. Burg,[a] Steven Bruner,[a] Elisabetta Brenna,[b] Adrian E. Roitberg[a] and Jon D. Stewart *[a]

Received 2nd March 2018,
Accepted 28th August 2018

DOI: 10.1039/c8cy00440d

rsc.li/catalysis

Saccharomyces cerevisiae OYE 3 shares 80% sequence identity with the well-studied *Saccharomyces pastorianus* OYE 1; however, wild-type OYE 3 shows different stereoselectivities toward some alkene substrates. Site-saturation mutagenesis of Trp 116 in OYE 3 followed by substrate profiling showed that the mutations had relatively little effect, opposite to that observed previously for OYE 1. The X-ray crystal structures of unliganded and phenol-bound OYE 3 were solved to 1.8 and 1.9 Å resolution, respectively. Both structures were nearly identical to that of OYE 1, with only a single amino acid difference in the active site region (Ser 296 *versus* Phe 296, part of loop 6). Despite their essentially identical static X-ray structures, molecular dynamics (MD) simulations revealed that loop 6 conformations differed significantly in solution between OYE 3 and OYE 1. In OYE 3, loop 6 remained nearly as open as observed in the crystal structure; by contrast, loop 6 closed over the active site of OYE 1 by *ca.* 4 Å. Loop closure likely generates a greater number of active site protein contacts for substrate bound to OYE 1 as compared to OYE 3. These differences provide an explanation for the differing stereoselectivities of OYE 3 and OYE 1, despite their nearly identical X-ray crystal structures.

Introduction

Since its discovery as the first cofactor-containing enzyme,[1] the old yellow enzyme from *Saccharomyces pastorianus*[2] (OYE 1) has been an important testbed for discovering general principles of flavoprotein structure and mechanism.[3–5] Biocatalytic interest in OYE 1 and its relatives grew rapidly after Massey's discovery that it reduces electron-deficient alkenes with very high stereoselectivity.[6] Over the past two decades, the substrate range of *S. pastorianus* OYE 1 has been explored extensively; in parallel, many homologs have been cloned, overexpressed and their synthetic abilities evaluated.[7–9] In addition, a number of protein engineering approaches have also been applied to OYE 1 and its homologs to improve substrate acceptance, alter stereoselectivity, *etc.*[10–14]

OYE 1-mediated alkene reductions proceed with net *trans*-addition of both hydrogen atoms, with hydride from reduced FMN adding to the substrate β-carbon lying above the cofactor and protonation from the opposite face of the alkene mediated by a Tyr side-chain (Scheme 1).[6] Substrate binding orientation thus dictates which face of the π system lies proximal to the flavin and thereby determines the absolute stereochemistry of the reduced product.

Fox and Karplus solved the X-ray crystal structure of OYE 1 in 1994;[15,16] since then, the structures of several OYE 1 homologs have been determined.[17–26] While all family members share a common TIM barrel architecture and have similar active site structures, the observation that some substrates bind in different orientations (and thus yield opposite stereoisomers) underscores the importance of small structural differences (for an early example, see ref. 27).

The genomes of both bakers' yeast (*Saccharomyces cerevisiae*) and brewers' bottom yeast (*S. pastorianus*) contain the OYE 1 gene.[28] The former also includes two homologs (OYE 2 and OYE 3).[29] All share very high mutual sequence identity.[30] To determine whether these minor sequence differences impacted stereoselectivity, we examined all published examples of alkene substrates that had been reduced by both OYE 1 and OYE 3. Unsurprisingly, the large majority of alkenes were reduced with the same stereopreferences;

[a] *Department of Chemistry, 126 Sisler Hall, University of Florida, Gainesville, FL 32611, USA. E-mail: jds2@chem.ufl.edu; Fax: +1 352 846 0743; Tel: +1 352 846 0743*

[b] *Dipartimento di Chimica, Materiali ed Ingegneria Chimica "Giulio Natta" Politecnico di Milano, Via Mancinelli 7, I-20131, Milano, Italy*

† Electronic supplementary information (ESI) available: Complete NMR spectra for ketones **3** and **4** along with their reduced products. See DOI: 10.1039/c8cy00440d

‡ These authors contributed equally to this work.

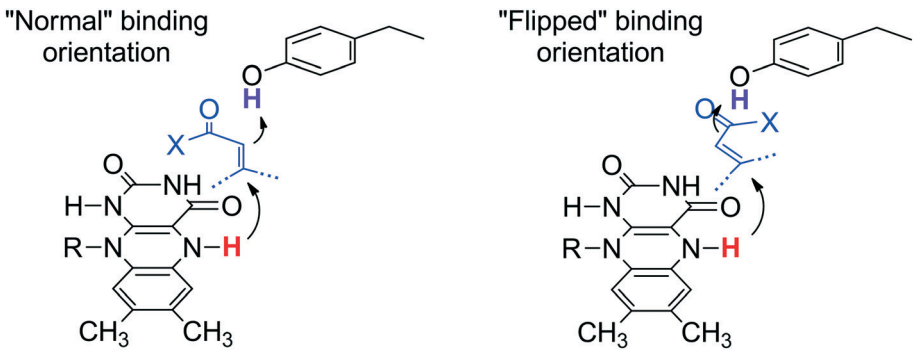

Scheme 1

however, five cases differed (Table 1). In each, the reaction outcomes suggested that all five bound to OYE 1 in the "normal" orientation (Scheme 1, left), but to OYE 3 in the "flipped" orientation (Scheme 1, right). Because three of these examples involve substrates of particular interest to our synthetic efforts,[31] we solved the X-ray crystal structure of *S. cerevisiae* OYE 3. We also explored the response of OYE 3 to mutations at Trp 116, a position that has proven highly influential in dictating the stereoselectivity of OYE 1.[32] Finally, we also carried out molecular dynamics simulations of both OYE 1 and OYE 3 to uncover possible differences in active site structure and dynamics that might help explain why reactions with OYE 3 sometimes differ from those of OYE 1.

Experimental

General

Restriction endonucleases, Phusion Hot Start II High-Fidelity DNA polymerase and T4 DNA ligase were purchased from New England Biolabs and primers were obtained from Integrated DNA Technologies. Crystallography screening kits (Classics Suite/AmSO$_4$ and PEGRx HT) were purchased from Qiagen and Hampton Research, respectively. All other reagents were obtained from commercial suppliers and used as received. Plasmids were purified on small scales by Wizard® minicolumns (Promega Life Sciences) and on large scales using CsCl density gradient ultracentrifugation. DNA sequencing was carried out by the University of Florida ICBR using capillary fluorescence methods using standard protocols. Growth media recipes have been described previously.[33]

Alkene substrates **5–19** were purchased from commercial suppliers or prepared in-house during previous studies.[34] Conversions and stereoselectivities were assessed by GC. Reactions of substrates **3** and **4** were analyzed on a 0.25 mm × 30 m HP-5MS column (Agilent) coupled with an MS detector to assess conversion, and on a 0.25 mm × 25 m Chirasil DEX CB column (Chrompack) coupled with an FID to assess enantioselectivity. Reactions of substrates **5**, **6**, **10** and **13–19** were analyzed on a 0.25 mm × 30 m Beta Dex 225 column (Astec) coupled with an FID. Reactions of alkenes **7–9** and **16** were analyzed on a 0.25 mm × 30 m DB-17 column (Agilent J&W) coupled with an MS detector. Temperature programs were tailored to provide baseline separations of each starting material and the corresponding product stereoisomers.

Determining the stereochemical courses of OYE 3 and OYE 1 reductions

Substrates **3** and **4** were prepared according to the literature.[35,36] Racemic samples of 4-methylhexan-3-one[37] and 4-methylheptan-3-one,[38] used as reference compounds, were prepared by hydrogenation of **3** and **4** on Pd/C in Et$_2$O. The absolute configurations of 4-methylhexan-3-one and 4-methylheptan-3-one, obtained by bioreduction, were established by comparison with optical rotation values reported in the literature.[39]

(*E*)-4-Methylhex-4-en-3-one 3. ^{1}H-NMR (CDCl$_3$, 400 MHz):[40] δ (ppm) 6.73 (1H, q, J = 6.9 Hz, *CH*═), 2.66 (2H, q, J = 7.3 Hz, CO*CH*$_2$CH$_3$), 1.85 (3H, d, J = 6.9 Hz, *CH*$_3$CH═), 1.78 (3H, s, *CH*$_3$C═), 1.09 (3H, t, J = 7.3 Hz, *CH*$_3$CH$_2$); ^{13}C-NMR (CDCl$_3$, 100.6 MHz):[40] δ (ppm) 202.5, 138.2, 136.7, 30.4, 14.8, 11.2, 9.0; GC-MS (EI) m/z (%) = 112 (M$^+$, 25), 83 (83), 55 (100).

(*E*)-4-Methylhept-4-en-3-one 4. ^{1}H-NMR (CDCl$_3$, 400 MHz):[41] δ (ppm) 6.61 (1H, t, J = 7.2 Hz, *CH*═), 2.68 (2H, q, J = 7.3 Hz, CO*CH*$_2$CH$_3$), 2.25 (2H, quintuplet, J = 7.3 Hz, *CH*$_2$-CH═), 1.78 (3H, s, *CH*$_3$C═), 1.13–1.03 (6H, m, *CH*$_3$CH$_2$CO and *CH*$_3$CH$_2$C═); ^{13}C-NMR (CDCl$_3$, 100.6 MHz): δ (ppm) 202.6, 143.4, 136.6, 30.4, 22.4, 13.2, 11.3, 8.9; GC-MS (EI) m/z (%) = 126 (M$^+$, 20), 97 (100), 69 (90).

4-Methylhexan-3-one. ^{1}H-NMR (CDCl$_3$, 400 MHz):[37] δ (ppm) 2.51–2.40 (3H, m, CO*CH*$_2$ + CO*CH*), 1.75–1.60 (1H, m, *CH*HCH$_3$), 1.45–1.33 (1H, m, *CH*HCH$_3$), 1.06 (3H, d, J = 7.0 Hz, *CH*$_3$CH), 1.05 (3H, t, J = 7.2 Hz, *CH*$_3$CH$_2$CO), 0.87 (3H, t, J = 7.6 Hz, *CH*$_3$CH$_2$CH); ^{13}C-NMR (CDCl$_3$, 100.6 MHz): δ (ppm) 215.4, 47.7, 34.4, 26.2, 16.1, 11.8, 7.9; GC-MS (EI) m/z (%) = 114 (M$^+$, 7), 86 (11), 57 (100).

4-Methylheptan-3-one. ^{1}H-NMR (CDCl$_3$, 400 MHz):[38] δ (ppm) 2.58–2.50 (1H, m, CO*CH*), 2.45 (2H, qd, J = 7.4 and 2.5 Hz, *CH*$_2$CH$_3$); 1.68–1.55 (1H, m, CH*CH*HCH$_2$), 1.38–1.20 (3H, m, CH*CH*HCH$_2$ + *CH*$_2$CH$_3$), 1.06 (3H, d, J = 7.0 Hz, *CH*$_3$CH), 1.04 (3H, t, J = 7.1 Hz, *CH*$_3$CH$_2$CO), 0.90 (3H, t, J = 7.6 Hz, *CH*$_3$CH$_2$CH$_2$); ^{13}C-NMR (CDCl$_3$, 100.6 MHz):[38] δ (ppm) 215.5, 46.0, 35.4, 34.3, 20.6, 16.5, 14.2, 7.9; GC-MS (EI) m/z (%) = 128 (5), 86 (49), 71 (74), 57 (100).

Table 1 Alkenes reduced by *S. pastorianus* OYE 1 and OYE 3 with differing stereoselectivities. All substrates are shown in the "normal" orientation and the phenol inhibitor skeleton is indicated by dashed grey lines. Products derived from a "flipped" substrate binding orientation are shown in red

Entry	Substrate	OYE 1 % ee	OYE 3 % ee	Ref.
1	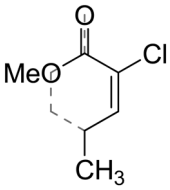	75% (*R*)	**59% (*S*)**	63
2	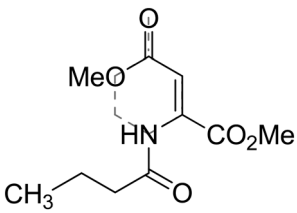	60% (*S*)[a]	**68% (*R*)**	64
3	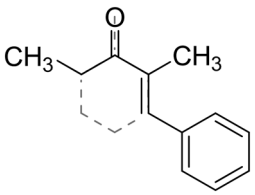	59% (*R*)	**89% (*S*)**	31
4	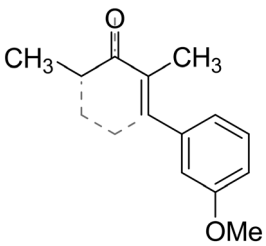	20% (*R*)	**95% (*S*)**	31
5	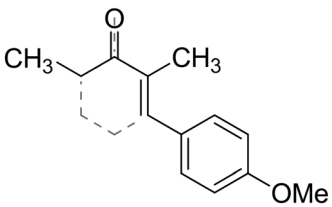	60% (*R*)	**81% (*S*)**	31

[a] The indicated binding orientations presume that the activating ester group was the same for both OYE 1 and OYE 3; however, a change in activating ester group would also be consistent with the observed data.

Enone **4** was submitted to bioreduction with NADPD using both OYE 3 and OYE 1 in D_2O. The substrate (50 μmol) dissolved in i-PrOH-d_8 (100 μL) was added to a KP_i buffer solution (5.0 mL, 50 mM in D_2O, pH 7.0) containing $NADP^+$ (15 μmol), *Thermoanaerobium brockii* alcohol dehydrogenase (4 U, 3 mg) and the required OYE (*ca.* 250 μg, dissolved in 500–700 μL H_2O). The mixture was incubated for 24 h in an orbital shaker (160 rpm, 30 °C). The solution was extracted with dichloromethane, centrifuging after each extraction, and the combined organic solutions were dried over anhydrous Na_2SO_4. ^2H spectra were recorded on a 400 MHz spectrometer with proton broad band decoupling, in $CHCl_3$ solutions, using $CDCl_3$ as internal reference for chemical shift scale.

Site-saturation mutagenesis of Trp 116 in OYE 3

Plasmid pRP4 (a derivative of pET 22b with an OYE 3 coding region flanked by *Nde*I and *Xho*I sites) was the template used to make OYE 3 Trp 116 site-saturation mutants. A pair of mutagenic primers containing a single codon replacement for Trp 116 was used to make each of the 19 mutants. PCR was performed in a total reaction volume of 50 μL, composed of 0.5 μL of template (18 ng μL^{-1}), 5 μL of both forward and reverse primers (5 mM), 1 μL of dNTP mix (10 mM), 10 μL of 5 × HF Phusion® Hot start buffer, 28 μL of sterile water, and 0.5 μL of Phusion® Hot Start II DNA Polymerase (2 U μL^{-1}). PCR involved an initial denaturation step at 98 °C for 30 s, followed by 25 cycles of denaturation at 98 °C for 10 s,

annealing at 64 °C for 30 s, and an extension step at 72 °C for 3 min 30 s, followed by a final extension step at 72 °C for 7 min 30 s.

PCR products were purified by Wizard® Plus SV Gel PCR Clean up kits (Promega) according to the manufacturer's instructions. The first aliquot of *Dpn*I (0.5 μL of a 20 U μL^{-1} stock) was added; after incubating for 4 h at 37 °C, a second aliquot of *Dpn*I was added and incubation was continued overnight at 37 °C. Digested PCR products were purified as before, then aliquots (4 μL) were used to transform 50 μL of *E. coli* ElectroTen-Blue cells (Agilent) using 2.5 kV. Immediately following electroporation, 600 μL of SOC medium was added and cells were incubated without shaking at 37 °C for 1 h, then plated onto LB plates supplemented with 200 μg mL^{-1} ampicillin. Plates were grown overnight at 37 °C. Plasmids were isolated from randomly-chosen colonies and sequenced to verify that the desired mutation was present, then aliquots (4 μL) were used to transform 80 μL of *E. coli* BL21-Gold(DE3) cells using electroporation (2.5 kV). Immediately after electroporation, 600 μL of SOC medium was added and cells were incubated without shaking at 37 °C for 45 min prior to plating onto LB plates supplemented with 200 μg mL^{-1} ampicillin. Plates were incubated overnight at 37 °C. Plasmids were isolated from each transformant and mutations were again verified by sequencing. The library was arrayed in a 96 well microtiter plate and cells were grown overnight at 37 °C in 600 μL of LB medium supplemented with 200 μg mL^{-1} ampicillin. Aliquots (120 μL) of each saturated culture were transferred to a new 96 well microtiter plate containing 30 μL of 80% glycerol (which yielded a final glycerol concentration of 15%). This master plate was stored at −80 °C.

Screening Trp 116 site-saturation mutagenesis library

E. coli BL21 (DE3) Gold cells harboring plasmids encoding wild-type and Trp 116 site-saturation OYE 3 mutants were shaken overnight at 250 rpm in a 96 well plate containing 600 μL of LB supplemented with 200 μg mL^{-1} ampicillin at 37 °C. Aliquots of each saturated culture (20 μL) were used to inoculate 2 mL wells of a square bottom 96 well plate that contained 600 μL of ZYP-5052 auto-induction medium[42] supplemented with 200 μg mL^{-1} ampicillin. Cultures were shaken overnight at 350 rpm and 37 °C in a locally-designed and fabricated aeration case.[43] Cells were harvested by centrifugation and then resuspended in 600 μL of reaction mixture (50 mM KP_i, 100 mM glucose, 15 mM alkene, pH 7.0). Reaction mixtures were shaken overnight at room temperature at 250 rpm prior to quenching with 500 μL of EtOAc. After thorough mixing, the organic phase was separated by centrifugation and removed for GC analysis.

OYE 3 purification and crystallogenesis

OYE 3 protein was purified as described in the ESI.† Fractions containing OYE 3 were pooled and concentrated by ultrafiltration to a final concentration of 40 mg mL^{-1} (using A^{280} and an estimated value of ε^{280} (76 905 M^{-1} cm^{-1})).[44]

Initial crystallization conditions were identified by screening with the PEGRX HT (Hampton Research) as well as the Classics Suite and $AmSO_4$ Suite (Qiagen) kits. Sitting drop vapor diffusion was used and wells contained 2 μL of crystallization solution and 2 μL of 20 mg mL^{-1} OYE 3 (in 50 mM Tris-Cl, 50 mM NaCl, pH 7.5). The best crystals were obtained after 14 days from well A8 of the PEG RX HT screening plate at room temperature and no further optimization of these crystallization conditions was required (50 mM MES monohydrate, 22% v/v PEG 400, 25 mM Tris, 25 mM NaCl, pH 8.0). Individual crystals were mounted and briefly soaked briefly in cryoprotection buffer (100 mM MES monohydrate, 22% v/v PEG 400, 15% (v/v) glycerol, pH 6.0) prior to flash cooling in liquid nitrogen for data collection.

Crystals were also grown from the well A10 conditions (PEG RX HT screening kit) using sitting drop vapor diffusion (2 μL of 100 mM sodium citrate tribasic dihydrate, 30% (v/v) polyethylene glycol monomethyl ether 550 crystallization solution and 2 μL of 20 mg mL^{-1} OYE 3 in 50 mM Tris-Cl, 50 mM NaCl, pH 7.5). Crystals grew after 10 days at room temperature. They were mounted in appropriately-sized loops, then soaked briefly in cryoprotection buffer (100 mM sodium citrate tribasic dihydrate, 30% (v/v) polyethylene glycol monomethyl ether 550, 2 15% (v/v) glycerol, pH 5.0) supplemented with with 2 mM *p*-hydroxybenzaldehyde. Samples were flash cooled in liquid nitrogen prior to synchotron data collection.

Data collection and structure refinement

All data sets were collected on the 21-ID-G beamline at the Advanced Photon Source, Argonne National Laboratory. Unsoaked and soaked crystals diffracted to maximum usable resolutions of 1.8 and 1.9 Å, respectively. Reflection data were processed using XDS.[45] Phases were obtained by molecular replacement (PHENIX)[46] using a modified *S. pastorianus* OYE 1 structure as the search model (PDB code 1OYB). All ligands and water molecules were removed prior to molecular replacement. The initial model was well defined throughout the scaffold of the protein except at the C-terminus, giving an R_{free} value of 0.37. Residues 398 and 399 (Lys and Asn, respectively) were poorly fit and these two positions were therefore initially deleted from the model. The initially calculated $2F_o - F_c$ and $F_o - F_c$ maps showed electron density patterns readily identifiable as FMN. After an initial simulated annealing refinement the R_{free} dropped to 0.31. Residues 398 and 399 were added to the model after the first round of refinement. Further refinement as well as continued cycles of model building using the structure validation tools in COOT[47] produced a final model with an R_{free} value of 0.22. Adding a chloride ligand in the active site accounted for most of the observed active site electron density in the unsoaked crystals. For the *p*-hydroxybenzaldehyde-soaked crystals, the ligand was readily identifiable by its electron density.

Molecular dynamics studies of OYE 3 and OYE 1

All simulations were performed using the AMBER16 suite.[48] The starting structure for OYE 1 was taken from the PDB (3TX9, 2.00 Å resolution) and the OYE 3 starting structure was from this study. The Amber ff14SB force field was used for the proteins and the parameters for the FMN cofactor were obtained from Bryce's group.[49] Starting topologies were built using the tleap module of AmberTools 16.[48] The systems were solvated in a 10 Å buffer of TIP3P water[50] using a truncated octahedral box under periodic boundary conditions. The SHAKE algorithm[51] was used to keep bonds involving H atoms at their equilibrium length and an 8 Å cutoff was applied for nonbonded interactions. Newton's equations[52] were integrated with a 4 fs time step, using hydrogen mass repartition[53] and frames were collected at 40 ps intervals. The collision frequency of the Langevin thermostat was 2 ps^{-1}. All simulations used different random seeds (ig = −1) to avoid synchronization artifacts.[54]

The initial structures were minimized for 5000 steps using steepest descent for the first 1000 cycles and switching to conjugate gradient, with 10 kcal mol^{-1} $Å^{-2}$ restraints applied to the backbone. Heating was done using a linear temperature gradient from 10 to 300 K during 0.8 ns at constant volume. Equilibration was performed at the final temperature during 8 ns using the same backbone restraints under NPT conditions. Finally, we performed 100 ns of free dynamics at a temperature of 300 K under NPT conditions. The simulations were done using GPU(CUDA) version of the pmemd.cuda module.[55] Five independent replicates of the molecular dynamics runs were done to gauge the reproducibility of the results obtained.

Results and discussion

Stereochemical courses of OYE 3- and OYE 1-mediated reductions

Our initial hypothesis for the stereochemical divergence between OYE 3 and OYE 1 was that the two enzymes bound substrates in opposite orientations. Ketones with the general structure of **1** are reduced by both OYE 3 and OYE 1 with (*S*)-selectivity; this might arise from a "flipped" substrate binding orientation in the active sites of both enzymes (Fig. 1A). When the α-substituent was lengthened by one methylene, *e.g.*, ketones **2** and Table 1, entries 3–5, reductions by OYE 3 and OYE 1 proceeded with divergent stereoselectivities (Table 1). This led us to test **3** and **4**, whose β-substituents (methyl and ethyl) are smaller than the aryl analogs investigated previously. Would such compounds behave similarly to ketone **2**, in spite of the reduced steric hindrance of the β-group?

Trisubstituted alkenes **3** and **4** were reduced by wild-type OYE 3 and OYE 1 with (*S*)- and (*R*)-stereoselectivities, respectively (Table 2), which imply "flipped" (OYE 3) and "normal" substrate binding orientations (OYE 1). The alternative explanation – that OYE 3 and OYE 1 followed different stereochemical courses in H_2 addition – was ruled out by reducing enone **4** with NADPD in D_2O.[56] In the ^1H NMR spectrum of the racemic hydrogenation product from **4**, the two protons at C_5 are characterised by different chemical shifts: one gives a multiplet in the range 1.67–1.25 (shown in blue), and the other occurs as a multiplet in the range 1.38–1. 20 (shown in red), which overlaps with the CH_2 in position 6 (Fig. 1B).

The ^2H NMR spectra of the two deuterated samples show that both OYE 3 and OYE 1 promote the addition of two deuterium atoms in the same stereospecific way, presumably *anti* in both cases (Fig. 1C). The deuterium atoms are characterized by the same chemical shift, 2.45 and 1.21 ppm, corresponding to the multiplets at 2.44 and 1.38–1.20 ppm observed in the ^1H NMR spectrum of racemic reduction product of **4**. No deuterium atom is present at the chemical shift corresponding to the proton shown in blue (Fig. 1B). These data demonstrate clearly that the reversal of stereoselectivity between OYE 3 and OYE 1 does *not* arise because of a change between net *anti*- and *syn*-addition of H_2, but rather is a consequence of substrate binding orientation in the active sites. Based on these results, we attempted to magnify differences in enzyme-substrate interactions between OYE 3 and OYE 1 by mutagenesis of Trp 116, which has a dramatic impact on binding orientation for some substrates in OYE 1.[32,57] Would changes at Trp 116 have the same impact on OYE 3? To answer this question, all possible variants at position 116 were created.[33]

Consequences of Trp 116 mutations in OYE 3 and OYE 1

We tested the Trp 116 mutant collections for both OYE 3 and OYE 1 (Table 2) against both **3** and **4**. In general, replacements for Trp 116 had relatively little impact in OYE 3, the sole exceptions being Phe for **3** and Leu, Met and Tyr for **4**, which increased the amount of (*R*)-product (although the overall stereoselectivity was near-racemic in all four cases). By contrast, it was possible to identify mutants with either good (*R*)- and (*S*)-stereoselectivities in the Trp 116 replacement library of OYE 1. These results showed that OYE 1 is far more sensitive to active site changes than OYE 3, suggesting that the active site of OYE 3 may have fewer protein-substrate contacts that dictate binding orientation.

In previous work, we observed that the "flipped" binding mode is most commonly observed with open chain trisubstituted alkenes.[58] Only when the G group is large relative to the α-substituent does the substrate adopt a "normal" binding orientation (Fig. 1D). In the case of **3** and **4**, however, the increased bulkiness of the ethyl (the G group) with respect to the methyl group (the α-substituent) promotes the "normal" binding mode in OYE 1, but not in OYE 3, as it was observed for ketone **2**, thus confirming that the hindrance of the β-group has little influence. Steric interactions between the G group and the residue at position 116 are much more important in OYE 1; by contrast, OYE 3 strongly prefers a "flipped" substrate binding orientation for trisubstituted alkenes, which cannot be overriden by changes to Trp 116.

To better define the importance of active site changes in OYE 3, the wild-type and all Trp 116 mutants were screened

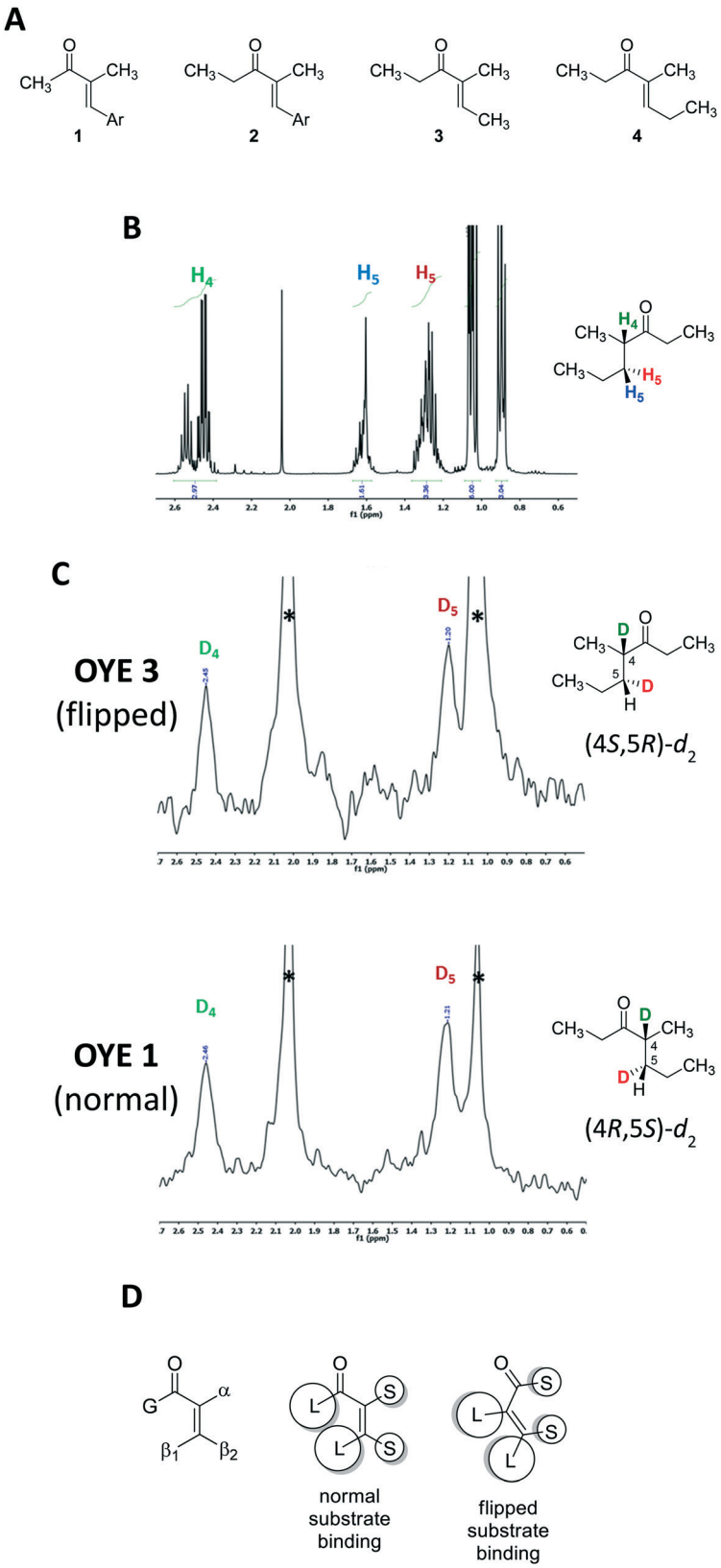

Fig. 1 Novel alkene substrates for OYE 3 and OYE 1. A. Trisubstituted alkenes **3** and **4** were designed as analogs of ethyl ketone **2** to test the sensitivity of OYE 3 and OYE to altered steric demands in the β-position. B. ^{1}H NMR spectrum of the racemic hydrogenated product from enone **4**. C. ^{2}H NMR spectrum of the (4*S*,5*R*)-d_2 product obtained by OYE 3-mediated reduction of ketone **4** in D_2O with NADPD (top) and the (4*R*,5*S*)-d_2 product obtained by OYE 1-mediated reduction of ketone **4** in D_2O with NADPD (bottom). The peaks labelled by an asterisk arise from acetone-d_6 and iso-propanol-d_8. D. Steric demands of trisubstituted alkene substrates of OYE 3 and OYE 1. The designations "L" and "S" refer to large and small substituents, respectively.

Table 2 Reductions of trisubstituted olefins by OYE 3 and OYE 1. Reactions that yield products from "flipped" substrate binding orientations are shown in red, and key results are highlighted by grey shading. In entry the first number refers to fractional conversion and the second to % ee

Amino acid at position 116	% c[a], % ee[b] 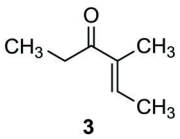 3		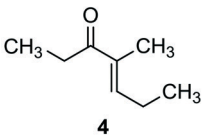 4	
	OYE 3	OYE 1	OYE 3	OYE 1
W (wt)	>98%, 78% (*S*)	>98%, 44% (*R*)	50%, 70% (*S*)	>98%, 56% (*R*)
A	82%, >99% (*S*)	**37%, 82% (*S*)**	—[c]	**5%, 58% (*S*)**
C	32%, 96% (*S*)	**40%, 70% (*S*)**	—	—
D	—	—	—	—
E	—	—	—	—
F	**32%, 14% (*R*)**	16%, 65% (*R*)	—	58%, >98% (*R*)
G	—	—	—	—
H	—	9%, 40% (*R*)	—	8%, 80% (*R*)
I	—	59%, 0%	—	64%, 50% (*R*)
K	—	—	—	—
L	>98%, 60% (*S*)	>98%, 50% (*R*)	**45%, 0%**	14%, 78% (*R*)
M	76%, 36% (*S*)	57%, 67% (*R*)	**47%, 0%**	78%, >99% (*R*)
N	35%, 74% (*S*)	33%, 34% (*R*)	10%, 46% (*S*)	11%, 64% (*R*)
P	—	9%, 88% (*R*)	—	—
Q	—	20%, 82% (*R*)	—	18%, >99% (*R*)
R	—	—	—	—
S	—	—	—	—
T	82%, >99% (*S*)	**9%, 67% (*S*)**	6%, 99% (*S*)	—
V	20%, >99% (*S*)	**>98%, 86% (*S*)**	31%, 96% (*S*)	**>98%, 54% (*S*)**
Y	25%, 76% (*S*)	11%, 78% (*R*)	**30%, 4% (*R*)**	>98%, 60% (*R*)

[a] Conversions were calculated on the basis of GC analysis of the crude mixture after 24 h reaction time (three replicates). [b] Optical purities were calculated from chiral-phase GC analysis (three replicates). [c] ≤5% substrate conversion after 24 h was observed.

against 15 alkene substrates that we had investigated in previous studies of OYE 1 using the same series of mutants (Fig. 2).[32,34,57]

Wild-type OYE 3 was unable to reduce Baylis–Hillman adduct **5**; by contrast, wild-type OYE 1 provides the reduction product from a "flipped" binding orientation with 60% ee (Table 3).[57] For both OYE 3 and OYE 1, all Trp 116 variants reduced **5** from a "normal" substrate binding orientation. A higher proportion of OYE 1 mutants retained catalytic activity toward **5** as compared to OYE 3, although all stereoselectivities were consistently (*S*).

2-(Hydroxymethyl)cyclohexenone **6** provided an interesting contrast between OYE 3 and OYE 1. While nearly all Trp 116 variants gave consistent (*S*)-stereoselectivities, Glu at position 116 of OYE 3 and OYE 1 yielded very different results (Table 3). In the sequence context of OYE 3, the Trp 116 Glu mutant provided a nearly racemic mixture from Baylis–Hillman adduct **6** (2% ee favoring the (*R*)-enantiomer). The analogous OYE 1 mutant gave the (*S*)-product in 90% ee, consistent with all other Trp 116 variants in the sequence context of OYE 1.

Reductions of (*S*)- and (*R*)-carvone demonstrated even more clearly that altering Trp 116 in OYE 3 and OYE 1 did

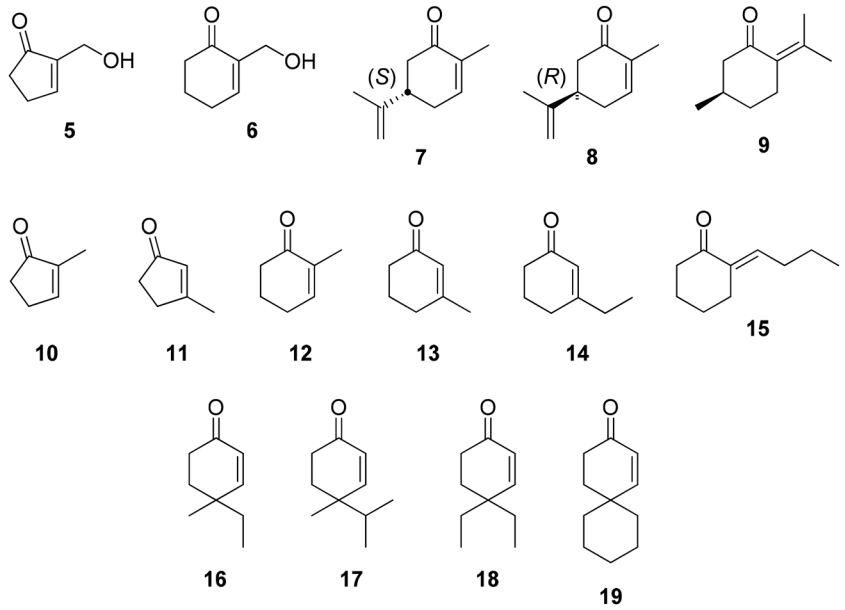

Fig. 2 Alkene substrates used to profile wild-type and Trp 116 site-saturation mutants of OYE 3.

not always yield the same results (Table 3). In the case of (*S*)-carvone **7**, the majority of substitutions for Trp 116 in OYE 1 prompted the alternative, "flipped" substrate binding mode.[32] This was not the case for OYE 3. In fact, none of the Trp 116 mutants triggered the "flipped" substrate binding mode. This was a highly unexpected result. (*R*)-Carvone **8** reductions also highlighted the subtle differences in active site behavior between OYE 1 and OYE 3. Two OYE 1 variants (Trp 116 Ala and Trp 116 Val) resulted in a predominantly opposite stereochemical course for (*R*)-carvone reduction;[32] however, the same two changes in an OYE 3 background led to a nearly 1 : 1 mixture of diastereomers, showing that Trp 116 mutations exert less control over substrate binding orientation in OYE 3 as compared to OYE 1.

Neither wild-type OYE 3 nor any Trp 116 variant reduced (*R*)-pulegone **9** or cyclopentenones **10** or **11** to significant extents. 2-Substituted cyclohexenone **12** was reduced by wild-type OYE 3, but it was not examined as a substrate for the Trp 116 variants. As expected,[59] sterically and electronically challenging 3-substituted cyclohexenones **13** and **14** were recalcitrant toward reduction by wild-type or any of the OYE 3 Trp 116 variants. While many of the OYE 3 Trp 116 mutants gave reasonable conversion for exocyclic enone **15** (with the Trp 116 Asn variant best), none yielded the opposite stereoisomer. The series of 4,4-disubstituted cyclohexenones **16–19** probed the ability of OYE 3 to accept bulky substituents in this portion of the substrate. Interestingly, while **16** and **17** were efficiently reduced by wild-type OYE 3 and all Trp 116 variants, none accepted **18** and **19**. While reductions of **16** and **17** might show kinetic resolutions, this point was not investigated since the starting enantiomers could not be separated by any of our available chiral GC columns; moreover, the achiral nature of the products makes any kinetic resolution only marginally useful.

Crystallographic studies of OYE 3

To help understand these differences in stereochemical outcomes, we solved the X-ray crystal structure of *S. cerevisiae* OYE 3. The protein was overexpressed in *E. coli* and purified by a phenol affinity resin[60] followed by gel filtration chromatography. After screening approximately 300 conditions, viable crystals were only observed when low molecular weight PEG was the main precipitant at near neutral pH values (pH 6). The most successful conditions yielded crystals that diffracted to a maximum usable resolution of 1.8 Å. The unit cell measured 61.2 × 107.8 × 141. 1 Å and the crystals belonged to space group $P2_12_12_1$ (Table 4). The asymmetric unit contained two protein molecules and a solvent content of 53.5%. A Matthews coefficient of 2.65 $Å^3$ Dal^{-1} was calculated.

The structure of OYE 3 was solved by molecular replacement (MR) using OYE 1 as the search model.[15] Successive rounds of refinement and model improvement yielded an R_{free} value of 0.22. The overall TIM barrel structure of OYE 3 is nearly identical to that of OYE 1 (overall rmsd = 0.26 Å using the 1OYB structure).

Once the protein scaffold was established, non-protein moieties were addressed. FMN was easily fit into the structure using the observed electron density. The flavin environment of OYE 3 parallels that of OYE 1, with amino acids Thr 37, Gly 72, Gln 114 and Arg 243 hydrogen positioned to form hydrogen bonds with the cofactor. The electron density in the vicinity of His 191 and Asn 194 was tentatively assigned to chloride as the predominant species. To help understand how substrates might interact with OYE 3, we solved the structure after briefly soaking with *p*-hydroxybenzaldehyde (Fig. 3A). This had essentially no change on the OYE 3 structure (apart from displacement of the active site chloride ligand). The phenolate oxygen lies between the side-chains of His 191 and Asn 194 and distances between the phenol and

Table 3 Trp 116 site-saturation mutagenesis data for OYE 3 and OYE 1. Reactions that yield products from "flipped" substrate binding orientations are shown in red, and key results are highlighted by grey shading

Amino acid at position 116	% ee				% de			
	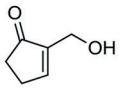 5		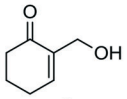 6		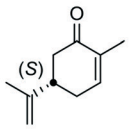 7		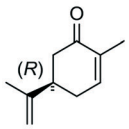 8	
	OYE 3	OYE 1[a]	OYE 3	OYE1[a]	OYE 3	OYE 1[b]	OYE 3	OYE 1[b]
W (wt)	—[c]	60% (*R*)	—	—	76% (*cis*)	90% (*cis*)	75% (*trans*)	97% (*trans*)
A	>98% (*S*)	72% (*S*)	>98% (*S*)	>98% (*S*)	—	93% (*trans*)	8% (*cis*)	56% (*cis*)
C	—	77% (*S*)	>98% (*S*)	>98% (*S*)	67% (*cis*)	73% (*trans*)	—	—
D	—	77% (*S*)	—	91% (*S*)	76% (*cis*)	>98% (*cis*)	75% (*trans*)	94% (*trans*)
E	23% (*S*)	88% (*S*)	2% (*R*)	90% (*S*)	84% (*cis*)	86% (*trans*)	78% (*trans*)	—
F	59% (*S*)	>98% (*S*)	>98% (*S*)	>98% (*S*)	81% (*cis*)	46% (*cis*)	66% (*trans*)	97% (*trans*)
G	>98% (*S*)	86% (*S*)	>98% (*S*)	>98% (*S*)	81% (*cis*)	93% (*trans*)	75% (*trans*)	—
H	71% (*S*)	77% (*S*)	78% (*S*)	>98% (*S*)	81% (*cis*)	75% (*cis*)	71% (*trans*)	96% (*trans*)
I	—	91% (*S*)	—	>98% (*S*)	83% (*cis*)	91% (*trans*)	88% (*trans*)	73% (*trans*)
K	—	76% (*S*)	—	>98% (*S*)	75% (*cis*)	—	73% (*trans*)	95% (*trans*)
L	70% (*S*)	57% (*S*)	>98% (*S*)	>98% (*S*)	67% (*cis*)	60% (*cis*)	60% (*trans*)	96% (*trans*)
M	>98% (*S*)	86% (*S*)	>98% (*S*)	>98% (*S*)	74% (*cis*)	78% (*trans*)	44% (*trans*)	89% (*trans*)
N	62% (*S*)	89% (*S*)	>98% (*S*)	>98% (*S*)	77% (*cis*)	70% (*trans*)	60% (*trans*)	69% (*trans*)
P	—	77% (*S*)	—	>98% (*S*)	79% (*cis*)	38% (*cis*)	79% (*trans*)	86% (*trans*)
Q	71% (*S*)	89% (*S*)	>98% (*S*)	>98% (*S*)	70% (*cis*)	82% (*trans*)	52% (*trans*)	47% (*trans*)
R	—	—	—	—	>98% (*cis*)	—	70% (*trans*)	—
S	—	>98% (*S*)	>98% (*S*)	>98% (*S*)	71% (*cis*)	>98% (*trans*)	68% (*trans*)	—
T	>98% (*S*)	>98% (*S*)	>98% (*S*)	>98% (*S*)	64% (*cis*)	85% (*trans*)	25% (*trans*)	—
V	53% (*S*)	92% (*S*)	>98% (*S*)	>98% (*S*)	43% (*cis*)	>98% (*trans*)	6% (*trans*)	56% (*cis*)
Y	73% (*S*)	87% (*S*)	>98% (*S*)	>98% (*S*)	81% (*cis*)	>98% (*cis*)	71% (*trans*)	>98% (*trans*)

[a] Ref. 57. [b] Ref. 32. [c] ≤10% substrate conversion after 24 h was observed.

protein residues for OYE 3 are very close to those observed previously for the analogous OYE 1 complex.[15]

All active site residues were identical between OYE 3 and OYE 1, except for position 296 (Ser in OYE 3 and Phe in OYE 1), located within loop 6 (residues 289–309). In native (unsoaked) OYE 3 crystals, the electron density for all residues in loop 6 is very well-defined (Fig. 3B). This is also the case for OYE 3 crystals soaked with *p*-hydroxybenzaldehyde (Fig. 3C), although three solvent-exposed Glu side-chains showed somewhat weak electron density beyond C_β.

Structural comparison of OYE 3 and OYE 1

As expected from their high sequence identity, the overall structures of OYE 3 and OYE 1 are highly similar. Even loop 6, which contains the only active site change (Ser 296 in OYE 3 and Phe 296 in OYE 1), was found in the essentially the same conformation for OYE 3 (in both ligand-soaked and unsoaked crystals) as well as in ligand-soaked crystals of OYE 1 (Fig. 4). The only significant difference between OYE 3 and OYE 1 *in crystallo* is the rotameric preference of the side-chains at position 296. In OYE 1, Phe 296 extends into the active site; in OYE 3, its side-chain is directed outward toward the solvent (Fig. 4).

Computational studies of OYE 3 and OYE 1

Since substrate binding orientation was the key to dictating stereoselectivity, we used the relevant crystal structures to model Michaelis complexes for all five substrates in Table 1

Table 4 Summary of X-ray crystallography data

Structure title	Wild-type OYE 3	*p*-HBA-soaked OYE 3
PDB ID	5V4V	5V4P
Ligand soaked	none	*p*-Hydroxybenzaldehyde
X-ray source	21-ID-G beamline APS Argonne National Laboratory	21-ID-G beamline APS Argonne National Laboratory
Space group	$P2_12_12_1$	$P2_12_12_1$
Unit cell dimensions *a*, *b*, *c* (Å)	61.2 107.8 141.1	61.5 106.4 141.0
Resolution (Å)	38.9–1.80 (1.86–1.80)[a]	24.9–1.88 (1.95–1.88)
Unique reflections	87 273(8428)	76 003(7463)
Completeness %	99.8(97.8)	100(99.8)
Multiplicity	14.5(14.3)	14.6(14.7)
$CC_{1/2}$	0.999(0.964)	0.999(0.978)
$I/\sigma(I)$	20.2(3.95)	18.6(5.36)
R_{work}	0.148(0.230)	0.181(0.205)
R_{free}	0.189(0.269)	0.219(0.251)
Ramachandran statistics		
Favored (%)	97	97
Allowed (%)	2.7	3.2
Outliers (%)	0	0
Number of protein, solvent, and ligand atoms	6396, 930, 92	6325, 396, 126
Average B factors (Å^2)	21.6	18.5
Protein	20.1	18.2
Ligands	22.4	25.1
Solvent	32.5	22.3

[a] Values in parentheses denote data for the highest resolution bin.

into the active sites of OYE 3 and OYE 1. Each was modeled separately in the "normal" and "flipped" orientations. This approach had been successful in understanding the stereopreferences in OYE 1 and other homologs.[43] For both enzymes, the "normal" substrate binding mode was easily modeled by overlaying the dashed lines with the *p*-hydroxybenzaldehyde bound to the active sites (Table 1). In the models of "flipped" substrate binding, the phenolic oxygen of *p*-hydroxybenzaldehyde and the *meta*-ring carbon marked the approximate locations of the carbonyl oxygen and β-carbon of the substrates, respectively (Scheme 1). In all cases, the substrate positions were consistent with angle and distance values observed for efficient hydride transfer from reduced FMN to C_β,[61] supporting the notion that these modeled structures might mirror catalytically productive complexes. Key protein-substrate distances were measured to identify possible steric interactions that would influence the choice "normal" *versus* "flipped" substrate binding.

Unfortunately, the modeled Michaelis complexes utterly failed to uncover any explanations for the differences in stereopreferences between OYE 3 and OYE 1. In fact, our models based on the X-ray structures predicted (incorrectly) that both enzymes would give entirely consistent outcomes, contradicting the experimental observations.

Because the active sites of OYE 3 and OYE 1 differ at position 296, and this residue lies on mobile loop 6, we considered the possibility that these proteins might possess different conformational and/or dynamic properties in solution that were not apparent in the X-ray structures. Each crystal structure was used as the starting point for MD simulations in the absence of substrate. Over the course of the simulations, variations in loop 6 conformations were observed; however, the average structures were well-defined (Fig. 5A and B). While both proteins showed approximately the same level of conformational mobility during the simulations, the average structure of loop 6 was more closed in OYE 1 as compared to OYE 3. This can be seen in the distance distributions between the C_α of residue 296 and the site of hydride addition (N_5 of the FMN) (Fig. 5C). In the starting X-ray structures of OYE 3 and OYE 1, these atoms are 10.1 and 9.9 Å apart, respectively. The MD simulation shows that in solution, loop 6 of OYE 1 closes significantly since the $C_{\alpha,296}$–$N_{5,FMN}$ distance decreased to approximately 7 Å. By contrast, loop 6 in OYE 3 failed to close over the active site – in fact, the $C_{\alpha,296}$–$N_{5,FMN}$ distance actually *increased* slightly to *ca.* 11 Å (Fig. 5D). The more open conformation of loop 6 over the active site of OYE 3 likely means that it has negligible contact with bound substrates, which would lessen its impact on stereoselectivity. Based on these results, we anticipate that the significantly altered loop 6 conformation in OYE 1, which is largely absent in OYE 3, is the major reason for the stereochemical differences that have been observed between these two enzymes (Table 1).

In the crystal lattices, loop 6 in both OYE 3 and OYE 1 faces a solvent channel, and there are no close contacts with symmetry-related protein molecules. Thus, the nearly identical loop 6 conformations observed *in crystallo* for these two proteins are *not* likely to be due to crystal packing forces. As noted above, the electron density for loop 6 is very well-defined in both the OYE 3 and OYE 1 structures and B-factors in this region are nearly the same as for other surface loops. Only by carrying out MD simulations in solution did the conformational differences become apparent.

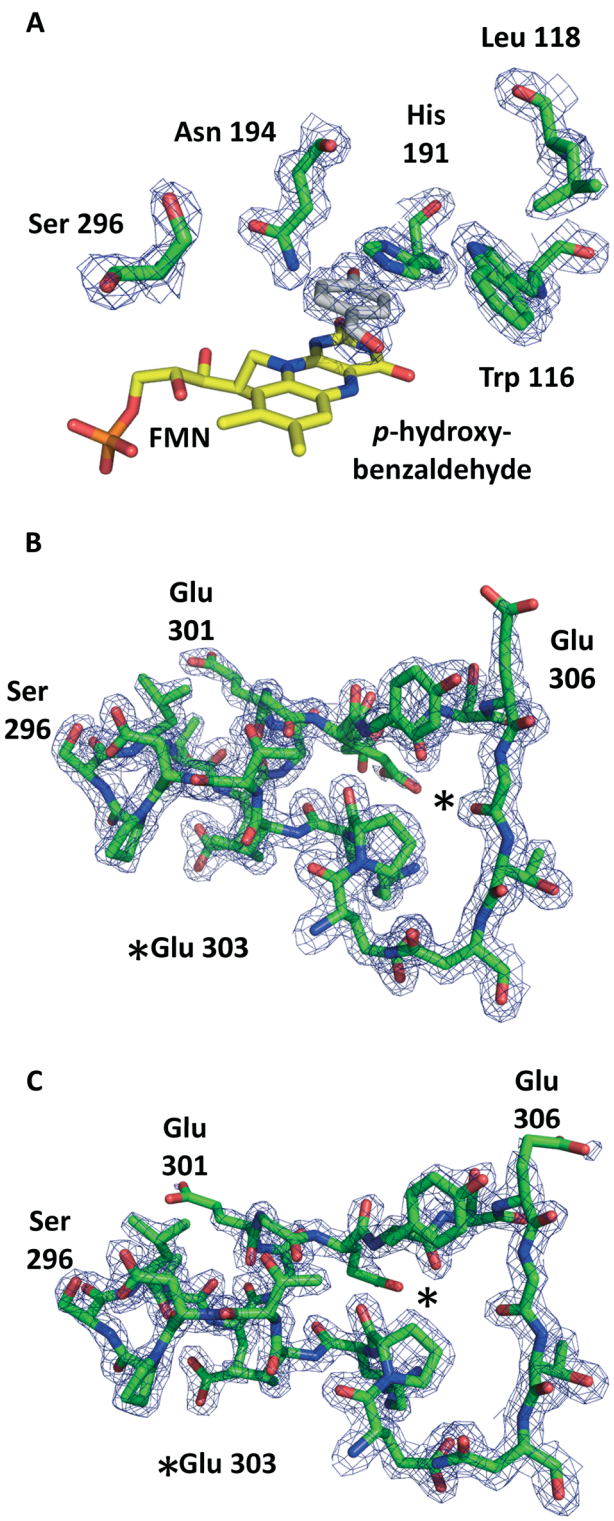

Fig. 3 OYE 3 crystal structure. Electron density ($2mF_o - DF_c$) is shown at the 1.5σ level. A. Active site structure of crystals soaked with *p*-hydroxybenzaldehye. The positions of key residues are shown. B. Loop 6 region (residues 289–309) of unsoaked OYE 3 crystals. Weak electron density was observed for the side-chain of Glu 303. C. Loop 6 region of OYE 3 crystals soaked with *p*-hydroxybenzaldehyde. Weak electron density was observed beyond the C_β carbons for Glu 301, Glu 303 and Glu 306.

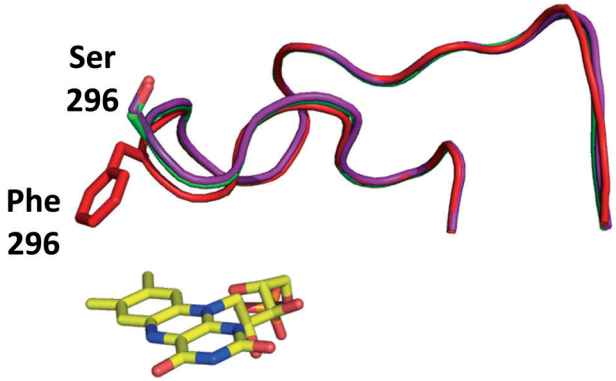

Fig. 4 Structural alignment of loop 6 regions for unsoaked OYE 3 crystals (purple), OYE 3 crystals soaked with *p*-hydroxybenzaldehyde (green) and OYE 1 crystals soaked with *p*-hydroxybenzaldehyde (red). Distances from the C_α of residue 296 to N_5 of FMN are *ca.* 10 Å in all cases.

That loop 6 is more closed over the active site in OYE 1 *versus* OYE 3 is also consistent with the stereochemical behavior of the two enzymes. In general, OYE 1 provides greater chiral discrimination, and changes elsewhere in the active site, *e.g.*, position 116, had large impacts on stereoselectivity. By contrast, the lessened ability of loop 6 to close over the OYE 3 active site yields a more open cavity with multiple opportunities for non-productive enzyme-substrate complexes to form. Moreover, this means that contacts with other amino acid side-chains will have lessened ability to influence substrate binding, as observed in this study.

Finally, the results from circular permutation studies of OYE 1 by the Lutz group are also consistent with our observations here.[13,62] The largest increases in catalytic efficiency (≥10-fold) occurred when the new termini dissected loop 6, which created an effectively "permanently open" loop 6. Interestingly, this group also found that mutating Trp 116 in the most catalytically efficient circular permutants had little impact on the stereoselectivity of (*S*)-carvone reduction, reminiscent of our observations on OYE 3. In both cases, loop 6 occupies a more open conformation than that found in wild-type OYE 1.

Conclusions

The conformation of loop 6 in *S. pastorianus* OYE 1 likely has a different structure in solution than that observed in its crystal structure. In solution, loop 6 of OYE 1 closes down over the active site, allowing it to interact closely with bound substrates and exert significant control over their binding orientations. By contrast, loop 6 in *S. cerevisiae* OYE 3 largely retains its crystallographically observed conformation in solution. Because the loop does not close over the active site of OYE 3, there are fewer protein – substrate contacts and substrate binding is less impacted by residues on this loop and elsewhere in the active site, *e.g.*, Trp 116. The divergent conformational preferences of loop 6 in OYE 1 and OYE 3 in solution may explain their differing stereochemical preferences

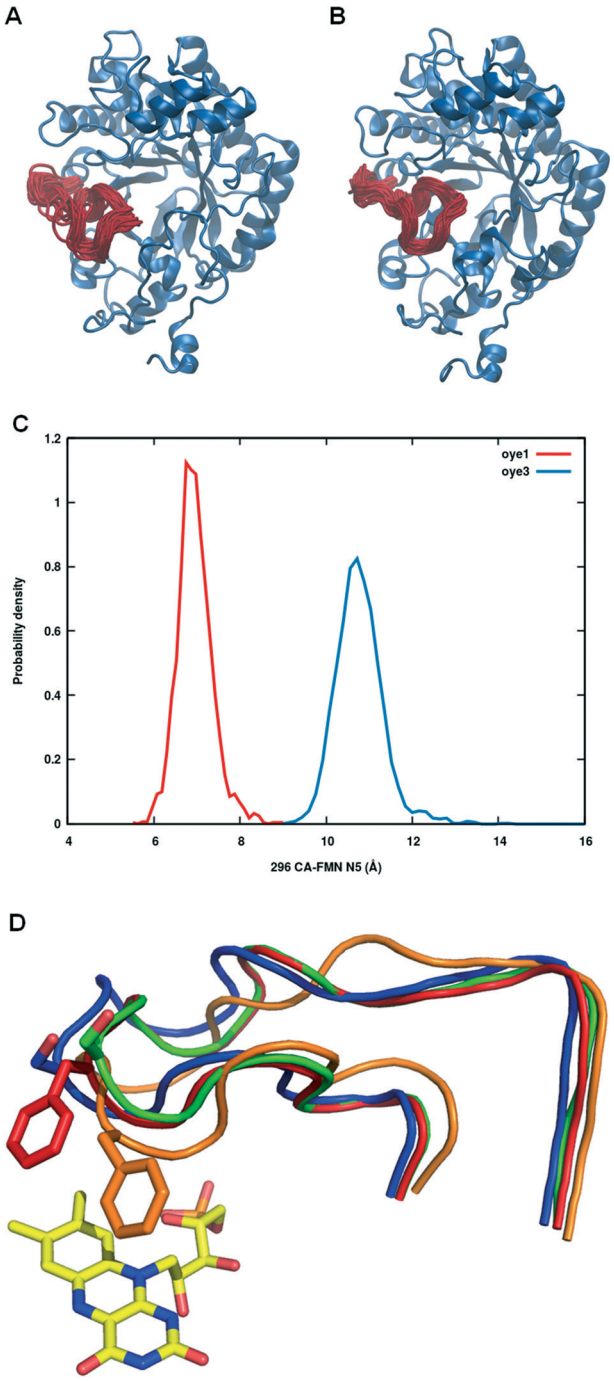

Fig. 5 MD simulation results for OYE 3 and OYE 1. A. Overlaid snapshots from a 100 ns simulation of OYE 3. Loop 6 is colored red and is the only portion of the protein structure that undergoes significant movement. B. Overlaid snapshots from a 100 ns simulation of OYE 1 in the absence of substrate. Loop 6 is colored red. C. Distances between the C_α of residue 296 and N_5 of FMN measured during MD simulations of OYE 3 (blue) and OYE 1 (red) in the absence of substrate. D. Overlaid protein structures; only the loop 6 regions are shown: OYE 3 X-ray structure (green), OYE 3 average coordinates after MD simulation (blue), OYE 1 X-ray structure (red), OYE 1 averaged coordinates after MD simulation (orange).

toward some substrates, despite the two proteins sharing 80% sequence identity and nearly the same crystal structures.

Whether the loop 6 conformations of OYE 3 and/or OYE 1 can be further impacted by additional mutations must await future experimental and computational studies that are currently underway. While in principle, mutating Ser 296 to Phe in OYE 3 might be expected to yield a variant with properties identical to OYE 1, a number of other residues differ between OYE 3 and OYE 1, and a single amino acid change may not be sufficient to effectively turn one protein into another. Only by examining a complete set of mutations and molecular dynamics trajectories will conclusions emerge. We also note that such altered structures might have very useful impacts on stereoselectivity, particularly when combined with additional active site changes. What has been clearly established by this work, however, is that static X-ray structures – while extremely useful – are not always sufficient to understand OYE-mediated alkene reductions.

Conflicts of interest

There are no conflicts of interest to declare.

Acknowledgements

We are very grateful for financial support from the National Science Foundation (CHE-1111791 and CHE-1705918). We would also like to thank Blue Waters (National Center for Supercomputing Applications) and the High Performance Computing Center (University of Florida) for providing computational resources.

Notes and references

1 O. Warburg and W. Christian, *Naturwissenschaften*, 1932, **20**, 980–981.
2 Formerly known as Saccharomyces carlsbergensis.
3 A. S. Abramovitz and V. Massey, *J. Biol. Chem.*, 1976, **251**, 5327–5336.
4 R. G. Matthews and V. Massey, *J. Biol. Chem.*, 1969, **244**, 1779–1786.
5 R. G. Matthews, V. Massey and C. C. Sweeley, *J. Biol. Chem.*, 1975, **250**, 9294–9298.
6 A. D. N. Vaz, S. Chakraborty and V. Massey, *Biochemistry*, 1995, **34**, 4246–4256.
7 M. Hall and A. S. Bommarius, *Chem. Rev.*, 2011, **111**, 4088–4110.
8 K. Durchschein, M. Hall and K. Faber, *Green Chem.*, 2013, **15**, 1764–1772.
9 H. S. Toogood and N. S. Scrutton, *Curr. Opin. Chem. Biol.*, 2014, **19**, 107–115.
10 D. J. Bougioukou, S. Kille, A. Taglieber and M. T. Reetz, *Adv. Synth. Catal.*, 2009, **351**, 3287–3305.
11 M. Hulley, H. S. Toogood, A. Fryszkowska, D. Mansell, G. M. Stephens, J. M. Gardiner and N. S. Scrutton, *ChemBioChem*, 2010, **11**, 2433–2447.

12 H. Toogood, A. Fryszkowska, M. Hulley, M. Sakuma, D. Mansell, G. M. Stephens, J. M. Gardiner and N. S. Scrutton, *ChemBioChem*, 2011, **12**, 738–749.
13 A. B. Daugherty, S. Govindarajan and S. Lutz, *J. Am. Chem. Soc.*, 2013, **135**, 14425–14432.
14 E. D. Amato and J. D. Stewart, *Biotechnol. Adv.*, 2015, **33**, 624–631.
15 K. M. Fox and P. A. Karplus, *Structure*, 1994, **2**, 1089–1105.
16 P. A. Karplus, K. M. Fox and V. Massey, *FASEB J.*, 1995, **9**, 1518–1526.
17 S. Horita, M. Kataoka, N. Kitamura, T. Nakagawa, T. Miykawa, J. Ohtsuka, K. Nagata, S. Shimizu and M. Tanokura, *ChemBioChem*, 2015, **16**, 440–445.
18 T. Barna, H. L. Messiha, C. Petosa, N. C. Bruce, N. S. Scrutton and P. C. F. Moody, *J. Biol. Chem.*, 2002, **277**, 30976–30983.
19 S. Reich, H. W. Hoeffken, B. Rosche, B. M. Nestl and B. Hauer, *ChemBioChem*, 2012, **13**, 2400–2407.
20 Y. A. Pompeu, B. Sullivan, A. Z. Walton and J. D. Stewart, *Adv. Synth. Catal.*, 2012, **354**, 1949–1960.
21 A. Fryszkowska, H. Toogood, M. Sakuma, G. M. Stephens, J. M. Gardiner and N. S. Scrutton, *Catal. Sci. Technol.*, 2011, **1**, 948–957.
22 D. J. Opperman, B. T. Sewell, D. Litthauer, M. N. Isupov, J. A. Littlechild and E. van Heerden, *Biochem. Biophys. Res. Commun.*, 2010, **393**, 426–431.
23 B. V. Adalbjörnsson, H. Toogood, A. Fryszkowska, C. R. Pudney, T. A. Jowitt, D. Leys and N. S. Scrutton, *ChemBioChem*, 2010, **11**, 197–207.
24 B. G. Fox, T. E. Malone, K. A. Johnson, S. E. Madson, D. Aceti, C. A. Bingman, P. G. Blommel, B. Buchan, B. Burns, J. Cao, C. Cornilescu, J. Doreleijers, J. Ellefson, R. Frederick, H. Geetha, D. Hruby, W. B. Jeon, T. Kimball, J. Kunert, J. L. Markley, C. Newman, A. Olson, F. C. Peterson, G. N. Phillips Jr., J. Primm, B. Ramirez, N. S. Rosenberg, M. Runnels, K. Seder, J. Shaw, D. W. Smith, H. Sreenath, J. Song, M. R. Sussman, S. Thao, D. Troestler, E. Tyler, R. Tyler, E. Ulrich, D. Vinarov, F. Vojtik, B. F. Volkman, G. Wesenberg, R. L. Wrobel, J. Zhang, Q. Zhao and Z. Zolnai, *Proteins: Struct., Funct., Bioinf.*, 2005, **61**, 206–208.
25 T. E. Malone, S. E. Madson, R. L. Wrobel, W. B. Jeon, N. S. Rosenberg, K. A. Johnson, C. A. Bingman, D. W. Smith, G. N. Phillips, Jr., J. L. Markley and B. G. Fox, *Proteins: Struct., Funct., Bioinf.*, 2005, **58**, 243–245.
26 K. Kitzing, T. B. Fitzpatrick, C. Wilken, J. Sawa, G. P. Bourenkov, P. Macheroux and T. Clausen, *J. Biol. Chem.*, 2005, **280**, 27904–27913.
27 M. Hall, C. Stueckler, B. Hauer, R. Stuermer, T. Friedrich, M. Breuer, W. Kroutil and K. Faber, *Eur. J. Org. Chem.*, 2008, 1511–1516.
28 K. Saito, D. J. Thiele, M. Davio, O. Lockridge and V. Massey, *J. Biol. Chem.*, 1991, **266**, 20720–20724.
29 K. Stott, K. Saito, D. J. Thiele and V. Massey, *J. Biol. Chem.*, 1993, **268**, 6097–6106.
30 OYE 1 and OYE 2 show 92.0% overall identity while OYE 1 and OYE 3 are 80.5% identical.
31 E. Brenna, S. L. Cosi, E. E. Ferrandi, F. G. Gatti, D. Monti, F. Parmeggiani and A. Sacchetti, *Org. Biomol. Chem.*, 2013, **11**, 2988–2996.
32 Y. A. Pompeu, B. Sullivan and J. D. Stewart, *ACS Catal.*, 2013, **3**, 2376–2390.
33 B. Sullivan, A. Z. Walton and J. D. Stewart, *Enzyme Microb. Technol.*, 2013, **53**, 70–77.
34 A. Patterson-Orazem, B. Sullivan and J. D. Stewart, *Bioorg. Med. Chem.*, 2014, **22**, 5628–5632.
35 D. Kalita, M. Morisue and Y. Kobuke, *New J. Chem.*, 2006, **30**, 77–92.
36 D. D. Faulk and A. Fry, *J. Org. Chem.*, 1970, **35**, 364–369.
37 H. C. Brown, R. K. Bakshi and B. Singaram, *J. Am. Chem. Soc.*, 1988, **110**, 1529–1534.
38 L. Wang, Z. Xu and T. Ye, *Org. Lett.*, 2011, **13**, 2506–2509.
39 For (*R*)-4-methylhexan-3-one in ref. 37, $[\alpha]_D^{23}$ = −30.8 (*c* 4, Et_2O); for (*R*)-4-methylheptan-3-one in ref. 38, $[\alpha]_D^{25}$ = −18 (*c* 1.5, hexane).
40 G. Sudhakar, J. Raghavaiah, G. Mahesha and K. K. Singarapuc, *Org. Biomol. Chem.*, 2016, **14**, 2866–2872.
41 J. Liu and S. Ma, *Org. Lett.*, 2013, **15**, 5150–5153.
42 F. W. Studier, *Protein Expression Purif.*, 2005, **41**, 207–234.
43 A. Z. Walton, *PhD thesis*, University of Florida, 2012.
44 *The Proteomics Handbook*, ed. S. Duvaud, M. R. Wilkins, R. D. Appel and A. Bairoch, Humana Press, Totowa, NJ, 2005.
45 M. D. Winn, C. C. Ballard, K. D. Cowtan, E. J. Dodson, P. Emsley, P. R. Evans, R. M. Keegan, E. B. Krissinel, A. G. W. Leslie, A. M. McCoy, S. J. McNicholas, G. N. Murshudov, N. S. Pannu, E. A. Potterton, H. R. Powell, R. J. Read, A. Vagin and K. S. Wilson, *Acta Crystallogr., Sect. D: Biol. Crystallogr.*, 2011, **67**, 235–242.
46 P. D. Adams, P. V. Afonine, G. Bunkoczi, V. B. Chen, I. W. Davis, N. Echols, J. J. Headd, L. W. Hung, G. J. Kapral, R. W. Grosse-Kunstleve, A. J. McCoy, N. W. Moriarty, R. Oeffner, R. J. Read, D. C. Richardson, J. S. Richardson, T. C. Terwilliger and P. H. Zwart, *Acta Crystallogr., Sect. D: Biol. Crystallogr.*, 2010, **66**, 213–221.
47 P. Emsley, B. Lohkamp, W. G. Scott and K. Cowtan, *Acta Crystallogr., Sect. D: Biol. Crystallogr.*, 2010, **66**, 486–501.
48 D. A. Case, R. M. Betz, W. Botello-Smith, D. S. Cerutti, T. E. Cheatham, T. A. Darden III, R. E. Duke, T. J. Giese, H. Gohlke, A. W. Goetz, N. Homeyer, S. Izadi, P. Janowski, J. Kaus, A. Kovalenko, T. S. Lee, S. LeGrand, P. Li, C. Lin, T. Luchko, R. Luo, B. Madej, D. Mermelstein, K. M. Merz, G. Monard, H. Nguyen, H. T. Nguyen, I. Omelyan, A. Onufriev, D. R. Roe, A. Roitberg, C. Sagui, C. L. Simmerling, J. Swails, R. C. Walker, J. Wang, R. M. Wolf, X. Wu, L. Xiao, D. M. York and P. A. Kollman, *AMBER*, University of California, San Francisco, 2016.
49 C. Schneider and J. Sühnel, *Biopolymers*, 1999, **50**, 287–302.
50 W. L. Jorgensen, J. Chandraskhar, J. D. Madura, R. W. Impey and M. L. Klein, *J. Chem. Phys.*, 1983, **79**, 926–935.

51 S. Miyamoto and P. Kollman, *J. Comput. Chem.*, 1992, **13**, 952–962.
52 J.-P. Ryckaert, G. Ciccotti and H. J. C. Berendsen, *J. Comput. Phys.*, 1977, **23**, 327–341.
53 C. W. Hopkins, S. Le Grand, R. C. Walker and A. E. Roitberg, *J. Chem. Theory Comput.*, 2015, **11**, 1864–1874.
54 D. J. Sindhikara, S. Kim, A. F. Voter and A. E. Roitberg, *J. Chem. Theory Comput.*, 2009, **5**, 1624–1631.
55 S. Le Grand, A. W. Götz and R. C. Walker, *Comput. Phys. Commun.*, 2013, **184**, 374–380.
56 NADPD was prepared in situ by the $NADP^+$-dependent oxidation of iso-propanol-d_8 using *Thermoanaerobium brockii* alcohol dehydrogenase.
57 A. Z. Walton, W. C. Conerly, Y. Pompeu, B. Sullivan and J. D. Stewart, *ACS Catal.*, 2011, **1**, 989–993.
58 E. Brenna, F. G. Gatti, A. Manfredi, D. Monti and F. Parmeggiani, *Catal. Sci. Technol.*, 2013, **3**, 1136–1146.
59 M. A. Swiderska and J. D. Stewart, *J. Mol. Catal. B: Enzym.*, 2006, **42**, 52–54.
60 A. S. Abramovitz and V. Massey, *J. Biol. Chem.*, 1976, **251**, 5321–5326.
61 M. W. Fraaije and A. Mattevi, *Trends Biochem. Sci.*, 2000, **25**, 126–132.
62 A. B. Daughterty, J. R. Horton, X. D. Cheng and S. Lutz, *ACS Catal.*, 2015, **5**, 892–899.
63 G. Tasnádi, C. K. Winkler, D. Clay, N. Sultana, W. M. F. Fabian, M. Hall, K. Ditrich and K. Faber, *Chem. – Eur. J.*, 2011, **18**, 10362–10367.
64 C. Stueckler, C. K. Winkler, M. Hall, B. Hauer, M. Bonnekessel, K. Zangger and K. Faber, *Adv. Synth. Catal.*, 2011, **353**, 1169–1173.

